Combustion and Flame 245 (2022) 112368

Contents lists available at ScienceDirect

Combustion and Flame

journal homepage: www.elsevier.com/locate/combustflame

On nanosecond plasma-assisted ammonia combustion: Effects of pulse and mixture properties

Mohammad Shahsavari[a,*], Alexander A. Konnov[b], Agustin Valera-Medina[c], Mehdi Jangi[a]

[a] Department of Mechanical Engineering, University of Birmingham, United Kingdom
[b] Division of Combustion Physics, Department of Physics, Lund University, Sweden
[c] College of Physical Science and Engineering, Cardiff University, United Kingdom

ARTICLE INFO

Article history:
Received 28 April 2022
Revised 30 August 2022
Accepted 1 September 2022

Keywords:
Ammonia combustion
Plasma-assisted combustion
Nanosecond-pulsed plasma discharge

ABSTRACT

In this study, the effects of nanosecond plasma discharges on the combustion characteristics of ammonia are investigated over a wide range of mixture properties and plasma settings. The results reveal that the impacts of the plasma on ammonia combustion change non-monotonically by altering the reduced electric field value. Within the studied range of the reduced electric field, i.e., 100–700 Td, it is shown that plasma is most effective in the medium range, e.g., 250–400 Td. At lower values, the main fraction of the plasma energy is consumed to excite the diluent to higher vibrational levels. At very high reduced electric field values, a substantial portion of the plasma energy is transferred into the ionization reactions of the diluent, which compromises the effective excitations of fuel and oxidizer species. In terms of the pulse energy density, results indicate that an increase in the range of 0–20 mJ/cm^3, at a given reduced electric field, decreases the ignition delay time by five orders of magnitude, and increases the laminar flame speed up to an order of magnitude, depending on the mixture composition. The results show that the plasma discharge produces more radicals, electronically excited and charged species when He is used as the diluent in the oxidizer instead of N_2, since NH_3 and O_2 ionization reactions are strengthened in NH_3/O_2/He. Moreover, plasma discharge is highly effective in assisting the combustion of preheated lean mixtures. The present study also indicates that ammonia flame thickness is minimum at a critical pulse energy density in the range of 12–14 mJ/cm^3. Further increases in the pulse energy density can manipulate the inner structure of the flame, altering the pre-heat zone of the flame to include some levels of chemical reactions toward the flameless mode of combustion.

1. Introduction

Ammonia is known as the low-hanging fruit for decarbonizing combustion in the industrial sectors, thanks to its high hydrogen content and energy density combined with its relatively simple production, storage, and shipping technologies [1]. Nevertheless, ammonia reactivity is considerably lower than typical hydrocarbon fuels, which makes it a daunting task to supplant widely used fuels with ammonia in conventional engines [1]. Currently, preheating and co-burning are considered the main approaches to improving ammonia reactivity [1,2]. However, co-burning (either as a dual or in a blend with other reactive fuels), compromises the advantages of ammonia as a carbon-free fuel if the second fuel is not hydrogen, an issue that seems likely for early system reconversions [2]. An alternative intriguing method would be to assist ammonia flames by plasma [3–5]. Compared to preheating, it has been shown that plasma discharge, at the same level of energy input, decreases the ignition delay time (IDT) of hydrogen/air mixtures by an order of magnitude [6]. In principle, plasma assists combustion through various routes including manipulating the mixture's thermophysical properties and kinetics of combustion [7]. Such impacts can also drastically change combustion characteristics as shown by Sun et al. that plasma converts the conventional S-shape ignition-extinction curve to a fully stretched monotonic curve in CH_4/O_2/He mixtures [8].

There are several types of plasma generators including a torch, gliding arc, nanosecond, and microwave discharges [3]. Among these, non-thermal/non-equilibrium nanosecond discharge (NSD) is known as the most energy-efficient technology [9,10]. All types of plasma-assisted combustion systems exhibit highly multiscale re-

* Corresponding author.
E-mail address: m.shahsavari@bham.ac.uk (M. Shahsavari).

https://doi.org/10.1016/j.combustflame.2022.112368

actions, ranging from microsecond chain propagation, termination, quenching, and ion-recombination reactions to picosecond electron impact reactions. However, unlike thermal reactions, electron impact reactions are independent of the gas temperature; hence, they can trigger both low and high-temperature pathways [6]. Recently, Faingold et al. performed zero-dimensional simulations to study IDT of stoichiometric NH_3/O_2/He and $NH_3/O_2/N_2$ mixtures assisted by plasma [4,5]. They showed that a limited number of low-energy NSD can reduce IDT of high-temperature mixtures by 40–60% [4]. They also showed that the number of pulses and pulse repetition frequency required to ignite the mixture increase drastically as the mixture temperature reduces [4]. Tianeja et al. showed that using plasma discharge can extend the flammability limits of NH_3/O_2/He mixtures [11]. Choe et al. presented a brief communication on the flame enhancement of NH_3/Air mixtures in which they observed experimentally that high-energy NSD lowers the lean blowout limit and NO_X emissions [12]. Lin et al. [13], Kim et al. [14], and Tang et al. [15] also confirmed that NOx emissions can be reduced in NH_3/Air flames by using high energy gliding arc plasma, dielectric barrier discharges, and AC powered gliding arc discharges, respectively. Moreover, Tianeja et al. and Jahnson et al. performed numerical simulations on plasma-assisted NH_3/air combustion [11,16]. They showed that ammonia oxidation pathways are dependent on the reduced electric field in the range of 150–550 Td [16]. However, the key chemical phenomena inducing such effects were not addressed in detail.

Despite the above-mentioned valuable community efforts, there are limited data and detailed analyses available in the literature on the effects of the reduced electric field, pulse energy density, equivalence ratio, diluent composition, and temperature on plasma-assisted ammonia combustion. Moreover, the majority of the previous studies were devoted to address the effects of plasma on the ignition delay time of ammonia, and no data is publicly available on the effects of plasma discharge on ammonia flame characteristics. To fill these gaps, the objective of the present study is to evaluate the impacts of nanosecond plasma discharge on the IDT and flame characteristics of ammonia over wide ranges of the reduced electric field, pulse energy density, and the mixture temperature and composition.

2. Numerical method and settings

2.1. Numerical solver

An open-source Boltzmann equation solver called ZDPlaskin [17] was coupled with in-house Cantera [18] codes. Each computational iteration involved a two-way coupling between ZDPlaskin and Cantera in which the electron impact equations were solved, and the results were passed on to Cantera for integrating the ODEs of thermal reactions. Here, the ignition delay time was calculated using an adiabatic constant-volume reactor, in which both plasma and thermal kinetics were solved over each time step. Furthermore, a one-dimensional freely propagating flame model was used to study the effects of plasma on unstrained premixed flame characteristics. To such an aim, first, fresh mixtures were stimulated by 20 nanosecond plasma pulses in an adiabatic constant-pressure reactor. Then, the output of this reactor was used as an input for the one-dimensional freely-propagating flame model. The pulse was modeled as a square wave as shown in Fig. 1. Here, an adaptive temporal resolution method was used to refine the time step during each pulse while minimizing the overall computational time. In this way, the chemical reactions during the plasma discharge were resolved using a time step of approximately 1×10^{-12} s, whereas the ODEs of thermal reactions were integrated using a timescale of 1×10^{-9} s. An example of the scheme used in this study can be found in Fig. 1.

2.2. Kinetic model

Preliminary studies, presented in the Supplementary Material, show that the mechanism developed by Han et al. [19] is an accurate and computationally efficient mechanism to predict ammonia combustion characteristics. Hence, this mechanism was used in the present study, which comprises 298 elementary reactions, including reactions of excited species, such as $O_2(a^1\Delta_g)$, $O(^1D)$, etc. introduced by Konnov [20]. The plasma kinetic mechanism was then assembled by incorporating the mechanism presented by Faingold et al. for NH_3/O_2/He [4] alongside the plasma reactions for N_2 from the study of Zhong et al. [21] with the collision cross sections for electron-species interactions obtained from LXCat database [22]. These allow to include excitations, ionizations, quenching, recombination, charge exchanges, and neutral state elementary reactions for $NH_3/O_2/N_2$/He mixtures into a unified mechanism.

2.3. Modeling parameters

The initial ammonia mixture temperature, T_{in}, and equivalence ratio, ϕ, were varied in the range of 298–1000 K, and 0.8–1.2, respectively. The mixture pressure was fixed at 1 atm. The amount of oxygen in O_2/N_2 and O_2/He was always 21%. The NSD settings were based on available plasma generators [23,24]. The plasma repetition frequency (*PRF*) was set at 50 kHz, while the reduced electric field, *E/N*, was varied in the range of 100–700 Td to find the most effective *E/N* to assist ammonia/air combustion. In each simulation, 20 pulses were discharged, which were shown to be sufficient for self-accelerating low-temperature chain branching reactions. Two ranges of NSD pulse energy density, E_p, were considered, one in the range of 0–1 mJ/cm^3 and the other 1–20 mJ/cm^3, with increments of 0.2 mJ/cm^3 and 1 mJ/cm^3, respectively. These are similar to the range that is typically used in literature. In previous studies, although low E_p values, i.e., $E_p < 1.3$ mJ/cm^3, were used to assist combustion of hydrocarbon fuels and ammonia [4,5,10,11,23,25,26], however, a relatively high E_p was required to reduce NOx emissions [13,15,27]. It is worth noting that increasing the number of pulses with low E_p values would result in similar reductions in NOx emissions as those with high E_p values, since both of these parameters control the amount of the plasma energy discharged into the mixture. Further investigations are needed to compare the effects of number of pulses and E_p on plasma-assisted ammonia combustion. The highest E_p value in the present study is limited to ensure that the mixture does not ignite prior to the discharging of 20 pulses. Here, an adaptive NSD pulse width, *w*, was employed, ensuring the specified E_p was released during each pulse. It should be mentioned that the pulse width is always less than 10 ns for the selected cases in this study, which is in the range of the ones used in the literature [4,11,16,27-30]. Here, simulations over the pulse width and between the pulses are denoted by “plasma phase” and “thermal phase” terms, respectively.

3. Validations

In the absence of publicly available detailed experimental data about the time history of species concentrations and temperature for ammonia combustion enhanced by using NSD, the solver was first validated by reproducing Faingold et al. numerical results on plasma-assisted NH_3/O_2/He ignition at $\phi = 1$ and $p = 1$ atm [4]. Fig. 1 shows the time history of the OH mole fraction and that of Faingold et al. [4]. Here, the initial number density of electrons was 1 cm^{-3}, without any electronically excited and charged species, “reactive plasma species”, or radicals as initial conditions. The predicted results are in good agreement with those of reference [4]. The lower OH mole fraction predicted in this

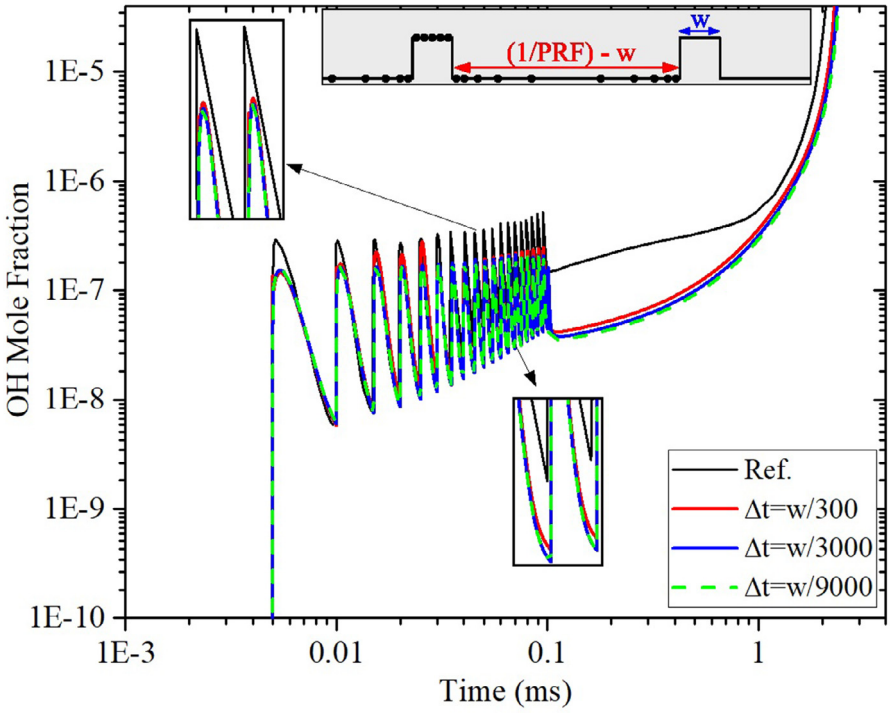

Fig. 1. Evolution of OH mole fraction in plasma assisted NH_3/O_2/He ignition for $\phi = 1$, $T_{in} = 1500$ K, $p = 1$ atm with $PRF = 200$ kHz and $E/N = 180$ Td.

study in the post-plasma phase, i.e., time > 0.1 ms, is consistent with the smaller peak values of OH during the pulses. This is not attributed to the numerical resolutions in the present simulations as here, the efforts were made to ensure sufficiently fine time steps, Δt, to obtain temporal resolution-independent results as can be seen in Fig. 1. It should be mentioned that details of the temporal resolution and the initial conditions are not fully provided in [4].

To further validate the numerical method, simulations were performed to reproduce the experimental data provided by Lefkowitz et al. on plasma-assisted CH_4/O_2/He combustion [31]. The kinetic mechanism developed by Mao et al. [32] was used to simulate plasma-assisted CH_4/O_2/He combustion in a constant-volume reactor. Fig. 2 shows the temporal evolution of temperature under 300 nanosecond plasma pulses. The instant of the last plasma discharge is shown by a vertical dash-dot line in Fig. 2. Here, the pulse repetition frequency is 30 kHz, and the reduced electric field is 180 Td. Similar modeling as the one used in reference [31] is utilized to include heat loss to the dielectrics. The uncertainty of the experimental data obtained by Lefkowitz et al. [31] is also shown in Fig. 2. Simulations were performed using different temporal resolutions to achieve resolution-independent data. The results show that the present numerical setup can well predict the temporal evolution of temperature under nanosecond plasma discharges.

4. Results and discussions

4.1. Reduced electric field in plasma-assisted ammonia combustion

Fig. 3 shows IDT and laminar flame speed of stoichiometric $NH_3/O_2/N_2$ at $T_{in} = 850$ K, $p = 1$ atm assisted by 20 nanosecond plasma pulses with $E_p = 5$ mJ/cm^3 as functions of E/N. The results show that both IDT and laminar flame speed change non-monotonically with E/N. This non-monotonic trend is in-line with the previously reported trends of the ignition delay time of plasma-assisted H_2/air [9], the fuel conversion in plasma-assisted CH_4 oxidation in the air [33], and ammonia oxidation in the air [16] as functions of E/N. Fig. 3 shows that plasma-assisted combustion has relatively low effectiveness at low E/N values, i.e., $E/N <$ 250 Td. Increasing the reduced electric field toward the medium range of E/N, i.e., 250 < E/N < 400 Td, significantly improves the effects of plasma on combustion. However, further increases in E/N slightly reduce the beneficial effects of the plasma discharge on the combustion characteristics.

More detailed studies on the effects of E/N on the plasma-assisted combustion are carried out by comparing the numerical results obtained for $E/N = 100$, 350, and 700 Td chosen as the representatives of the low, medium, and high reduced electric field values, respectively. Fig. 4 shows the percentage of the plasma energy taken by the electrons into different dominant excitation and ionization reactions as well as the main consumption path fluxes of a selected number of species in plasma-assisted ammonia/air combustion at $\phi = 1$, $T_{in} = 850$ K, $p = 1$ atm. Path fluxes were calculated during 20 plasma pulses. Further details of the branching of the plasma energy through the major reactions consuming the plasma energy are presented in the Supplementary Material. Fig. 4 shows that percentages of the plasma energy taken into the excitation reaction of O_2 and NH_3 are higher for $E/N = 350$ Td than the corresponding percentages in the cases with $E/N = 100$ or 700 Td. These excitation reactions produce NH_2, NH, H, and $O(^1D)$ radicals. The consumption path flux of $O(^1D)$ shown in Fig. 4 indicates that this species reacts with NH_3 and N_2 to generate OH, NH_2, and O radicals.

Considering the energy taken into the excitation and ionization reactions of N_2, the results show that the main part of the plasma energy, i.e., 46%, is used to excite the N_2 to the higher vibrational levels, i.e., v1-v8, for $E/N = 100$ Td. Such electronically excited species have negligible effects on the production of other reactive plasma species or radicals. Therefore, plasma energy is not used discreetly at low E/N values to produce effective reactive plasma species and radicals, e.g., O, H, OH, to assist ammonia combustion. This is demonstrated in Fig. 5 by plotting the maximum value of the mole fraction of the selected radicals and electronically excited

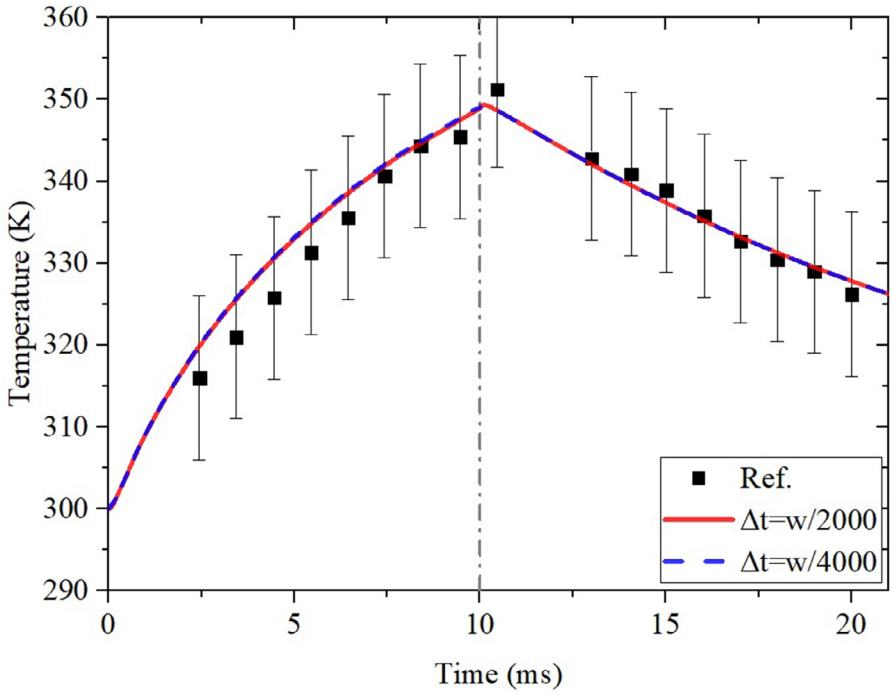

Fig. 2. Evolution of temperature in a stoichiometric CH_4/O_2 mixture with 75% dilution, (0.083 CH_4, 0.167 O_2, 0.75 He), for T_{in} = 300 K, p = 60 Torr under 300 plasma pulses with PRF = 30 kHz and E/N = 180 Td. Experimental reference data: Lefkowitz et al. [31].

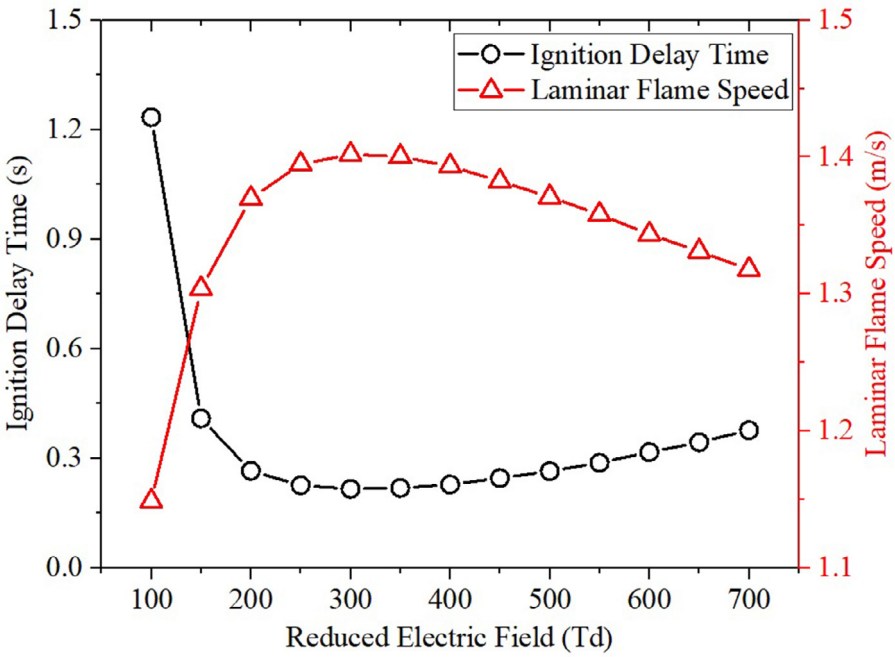

Fig. 3. Ignition delay time and laminar flame speed of plasma-assisted $NH_3/O_2/N_2$ combustion for ϕ = 1, T_{in} = 850 K with PRF = 50 kHz and E_p = 5 mJ/cm^3.

species during the plasma deposition averaged over 20 sequential pulses of the plasma deposition with E_p = 5 mJ/cm^3 in the stoichiometric $NH_3/O_2/N_2$ mixture. Contrary to this, at medium and high E/N values, the plasma energy is utilized to excite and ionize N_2 molecule to effectively assist combustion, while a negligible amount of the plasma energy is used to excite N_2 to the higher vibrational levels. Fig. 4 shows that 39.9% and 34.2% of the plasma energy, respectively for E/N = 350 and 700 Td, is taken by the electrons into the reactions to generate N_2(B), N_2(ab), N_2(C), and N(^{2}D) excited species. The path fluxes of these species show that all the above-mentioned electronically excited species react with O_2 and N_2 to generate other reactive plasma species and radicals, namely O, O(^{1}D), and O(^{1}S). Based on the above analyses, the plasma energy used in the excitation reactions of NH_3, O_2, and N_2 is higher for E/N = 350 Td than that used when E/N = 700 Td. Alternatively, the plasma energy transferred into N_2 ionization reactions, i.e., $e + N_2 \rightarrow 2e + N_2^+$, is higher for E/N = 700 Td than that for E/N = 350 Td. The path flux of N_2^+ shows that this ion reacts with the fuel to produce NH_3^+, which in turn absorbs electrons to generate NH_2, NH, and H radicals. The radical production via the diluent ionization route, being pronounced at high E/N values, comprises more elementary reactions, i.e., $e + N_2 \rightarrow 2e + N_2^+$,

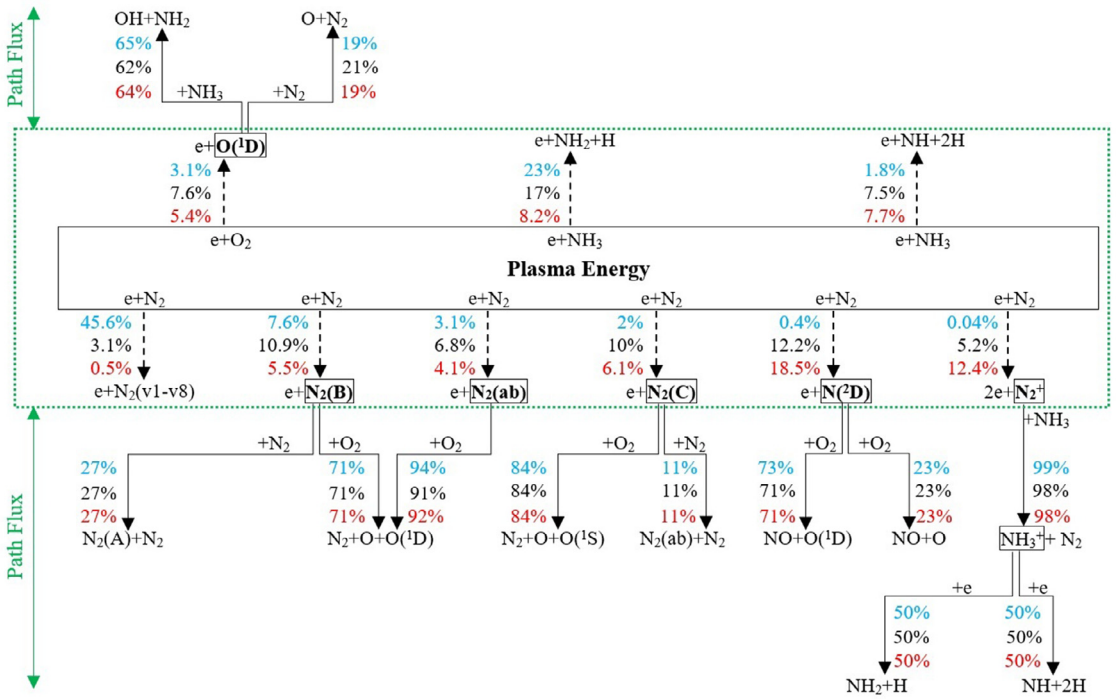

Fig. 4. Distribution of the plasma energy (dashed-arrows) as well as the consumption path flux (arrows) of a selected number of species (enclosed by rectangles) in plasma-assisted $NH_3/O_2/N_2$ combustion for T_{in} = 850 K, ϕ = 1.0 with *PRF* = 50 kHz and *E/N* = 100 Td (blue), 350 Td (black), and 700 Td (red). (For interpretation of the references to color in this figure legend, the reader is referred to the web version of this article.)

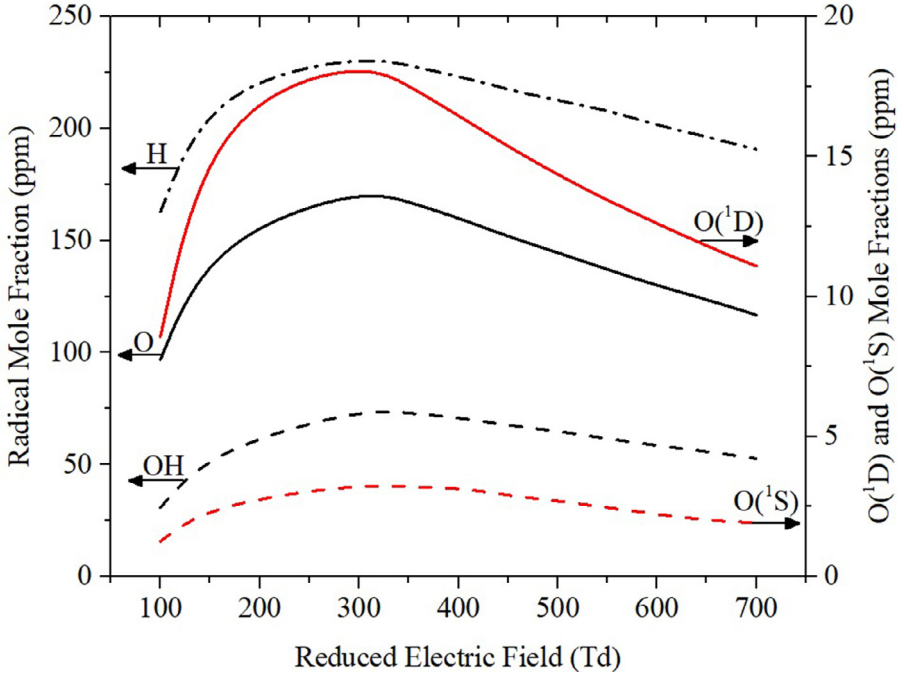

Fig. 5. Ensemble-averaged local maxima of mole fraction of O, H, OH, $O(^1D)$, and $O(^1S)$ in 20 sequential pulses of plasma discharge in $NH_3/O_2/N_2$ mixture at T_{in} = 850 K, ϕ = 1.0 with *PRF* = 50 kHz.

$N_2^+ + NH_3 \rightarrow NH_3^+ + N_2$, and $NH_3^+ + e \rightarrow NH_2$, NH, H, as those through the excitation reactions, e.g., $e + O_2 \rightarrow e + O(^1D)$, $O(^1D) + NH_3 \rightarrow OH$, NH_2. Besides, as it is shown in Fig. 5, compared with *E/N* = 700 Td, more OH radical is produced at *E/N* = 350 Td, e.g., via using more plasma energy to produce $O(^1D)$ which reacts with the fuel to produce OH radical. The more OH radicals, the quicker activation of the high-temperature reactions and subsequently faster ignition and flame propagation, as is observed in Fig. 3.

4.2. Effects of NSD on ignition delay time

Fig. 6 shows ammonia IDT in O_2/N_2 and O_2/He at T_{in} = 850 K, p = 1 atm and ϕ = 0.9–1.1. Increasing E_p strengthens the electron impact reactions during the plasma discharge, which subsequently raises the concentration of radicals and reactive plasma species, as well as the mixture temperature, which results in a considerable reduction of IDT. Fig. 7 shows the maximum value of the mole fraction of radicals, electronically excited, and charged

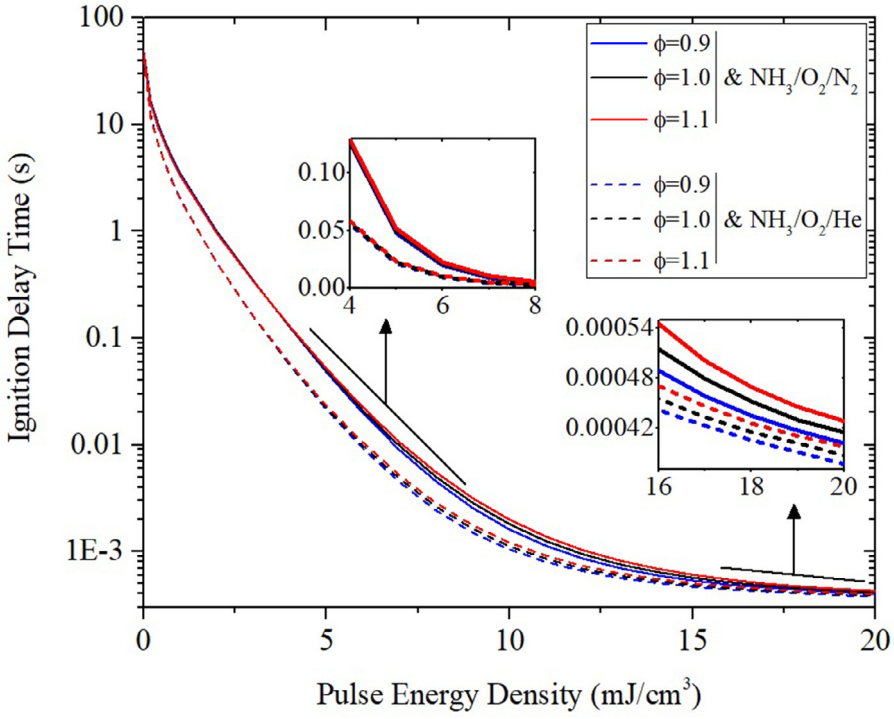

Fig. 6. IDT of $NH_3/O_2/N_2$ (solid lines) and NH_3/O_2/He (dash lines) as functions of E_p and ϕ for T_{in} = 850 K with *PRF* = 50 kHz and *E/N* = 350 Td.

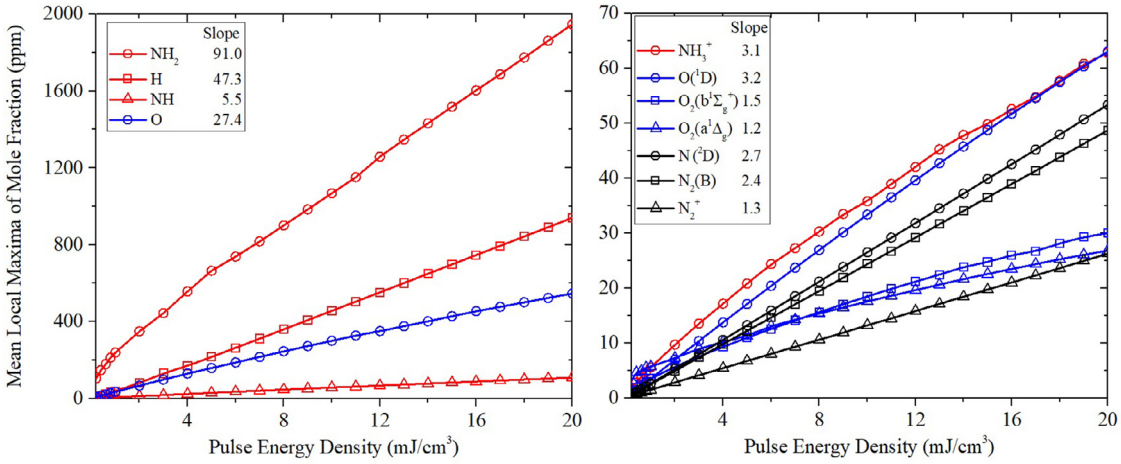

Fig. 7. Ensemble-averaged local maxima of mole fraction of radicals, electronically excited and charged species in 20 sequential pulses of plasma discharge in $NH_3/O_2/N_2$ mixture at T_{in} = 850 K, ϕ = 1.0 with *PRF* = 50 kHz and *E/N* = 350 Td.

species during the plasma deposition averaged over 20 pulses for the stoichiometric $NH_3/O_2/N_2$ mixture. The selected electronically excited and charged species are the most abundant ones generated by the plasma discharge for the present selected plasma settings. More details including the mole fraction of the minor reactive plasma species are presented in the Supplementary Material.

The results show that the mole fractions of the radicals and reactive plasma species generated by the NSD increase almost linearly by raising the E_p value. Linear curves are fitted into the data and the slopes of the fitted curves are presented in the legend, Fig. 7. The results also show that NSD with low E_p values (E_p < 3 mJ/cm^3), produces a considerable amount of $O_2(a^1\Delta_g)$. However, other electronically excited and charged species, i.e., NH_3^+, $O(^1D)$, $N(^2D)$, $N_2(B)$, and $O_2(b^1\Sigma_g^+)$, are significantly produced at higher E_p values. Increasing the pulse energy density noticeably enlarges the mole fractions of NH_2, H, and O radicals. It is worth noting that radicals are produced in both plasma and thermal phases. The plasma phase is the main source of radicals at low pulse energy densities, while at higher E_p values, the thermal phase plays the key role in generating radicals. For instance, path flux analyses show that 79% of H radical is generated by electron impact reactions in plasma-assisted stoichiometric $NH_3/O_2/N_2$ mixture at T_{in} = 850 K with E_p = 5 mJ/cm^3, while the corresponding value with E_p = 15 mJ/cm^3 is 31%. This is mainly because, unlike the cases with low E_p values, plasma discharges with a high pulse energy density produce large pools of reactive plasma species and radicals during the initial pulses, which in turn results in a rapid temperature augmentation. Subsequently, the thermal phase considerably contributes to generating the radicals between the underlying pulses.

Fig. 6 also shows that NSD is more effective in reducing the IDT of NH_3/O_2/He as compared with $NH_3/O_2/N_2$ for the selected plasma settings. Temporal evolutions of the electronically excited

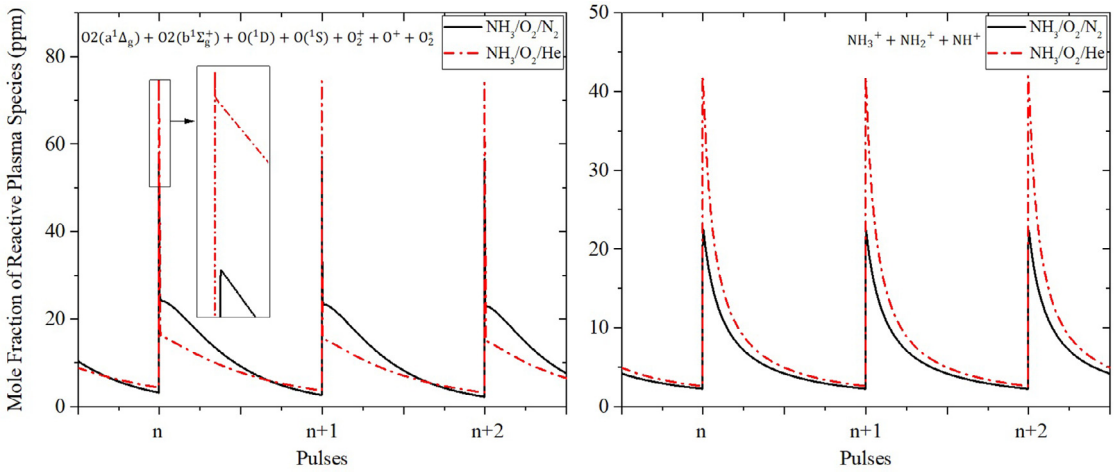

Fig. 8. Mole fractions of reactive plasma species in plasma-assisted $NH_3/O_2/N_2$ and $NH_3/O_2/He$ combustion for T_{in} = 850 K, ϕ = 1.0 with E_p = 5 mJ/cm^3, PRF = 50 kHz, and E/N = 350 Td.

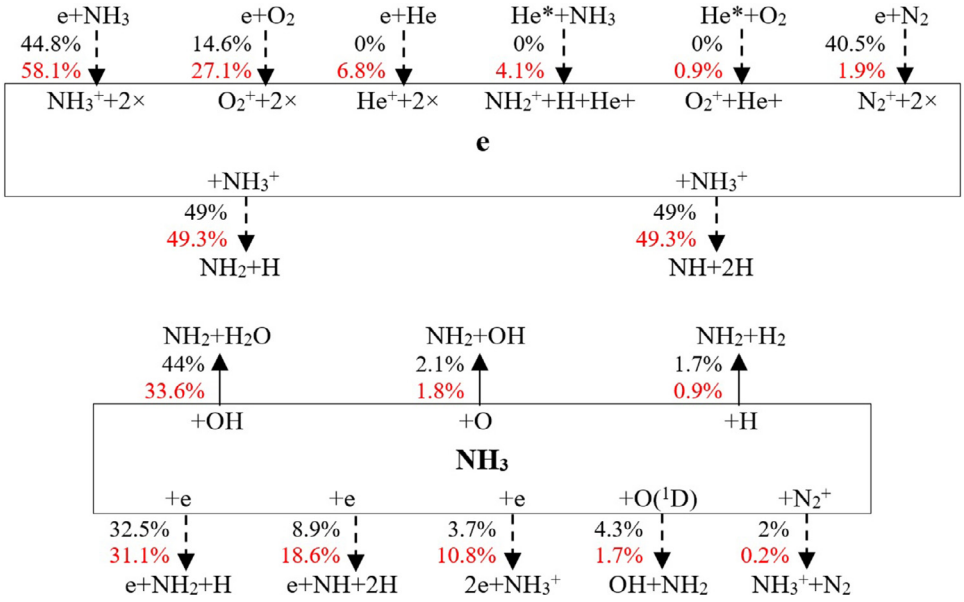

Fig. 9. Path fluxes of electron (top) and NH_3 (bottom) in plasma (dashed-arrows) and thermal (arrows) phases in plasma-assisted $NH_3/O_2/N_2$ (black) and $NH_3/O_2/He$ (red) combustion for T_{in} = 850 K, ϕ = 1.0 with E_p = 5 mJ/cm^3, PRF = 50 kHz, and E/N = 350 Td. (For interpretation of the references to color in this figure legend, the reader is referred to the web version of this article.)

and charged species plotted in Fig. 8 show that the diluent composition has noticeable effects on the production of the reactive plasma species. In Fig. 8, electronically excited and charged species originating from O_2 and NH_3 are calculated by taking the summation of {$O_2(a^1\Delta_g)$, $O_2(b^1\Sigma_g^+)$, O_2^+, O_2^*, $O(^1D)$, $O(^1S)$, O^+} and {NH_3^+, NH_2^+, NH^+}, respectively. The results show that NSD produces more reactive plasma species originating from NH_3 and O_2 during the pulses when N_2 is replaced by He. Fig. 8 also shows that the consumption rates of NH_3-originated charged species are almost identical in both cases. However, O_2 and O-charged and excited states are consumed faster in $NH_3/O_2/N_2$ as compared with $NH_3/O_2/He$ mixtures, since the slop of the corresponding carves is sharper between the pulses when N_2 is used as the diluent.

To further delineate the effects of the diluent composition on plasma-assisted ammonia combustion, the path fluxes of electron and NH_3 are plotted in Fig. 9. The fluxes were calculated over 20 plasma pulses discharged in the mixtures initiated at 850 K and 1 atm. The path flux of the electrons shows that the electrons are mainly produced during the electron impact reactions with NH_3 and O_2 rather than the diluent in $NH_3/O_2/He$, while a considerable amount of the electrons is generated during the diluent ionization in $NH_3/O_2/N_2$ mixture. Subsequently, ionization reactions produce more charged NH_3^+ and O_2^+ species in $NH_3/O_2/He$ as that in $NH_3/O_2/N_2$. This is consistent with the results presented in Fig. 8. The analyses also show that the ratios of the production and consumption rates of the electrons in $NH_3/O_2/He$ to the corresponding rates in the $NH_3/O_2/N_2$ mixture are 2.6 and 2, respectively. This indicates that the electrons are produced and consumed faster when N_2 is replaced in the oxidizer by He, which results in faster ionization reactions in the presence of He than that when N_2 is used as the diluent. Consequently, the fuel dissociates more in the plasma phase in $NH_3/O_2/He$ mixture than that in $NH_3/O_2/N_2$. The path flux of NH_3 shows that 64% of the fuel is dissociated during the plasma discharge in $NH_3/O_2/He$, while the corresponding value in $NH_3/O_2/N_2$ is 52%. The higher fuel dissociation in the plasma-assisted $NH_3/O_2/He$ mixture as those in $NH_3/O_2/N_2$ results in relatively faster OH radical production and consumption rates before the ignition, as it is shown in Fig. 10. In Fig. 10, the rates are calculated up to the instance of the ignition. The results show that the production rate of OH radical via H + $O_2 \leftrightarrow$OH+O reaction, as

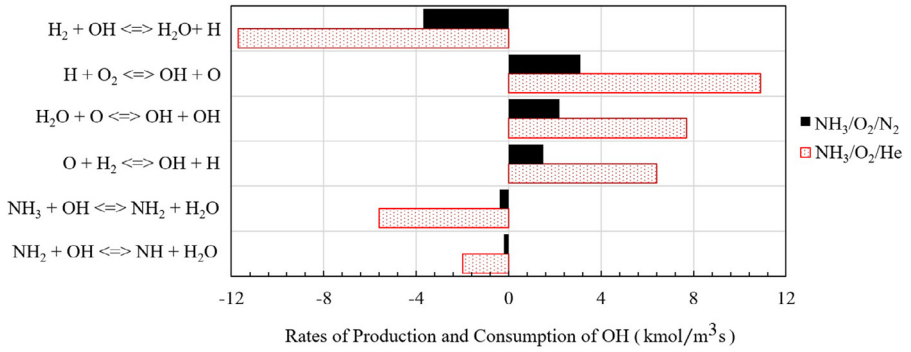

Fig. 10. Rates of production and consumption of OH radical in plasma-assisted $NH_3/O_2/N_2$ and NH_3/O_2/He combustion for T_{in} = 850 K and ϕ = 1.0 with E_p = 5 mJ/cm^3, *PRF* = 50 kHz, and *E/N* = 350 Td.

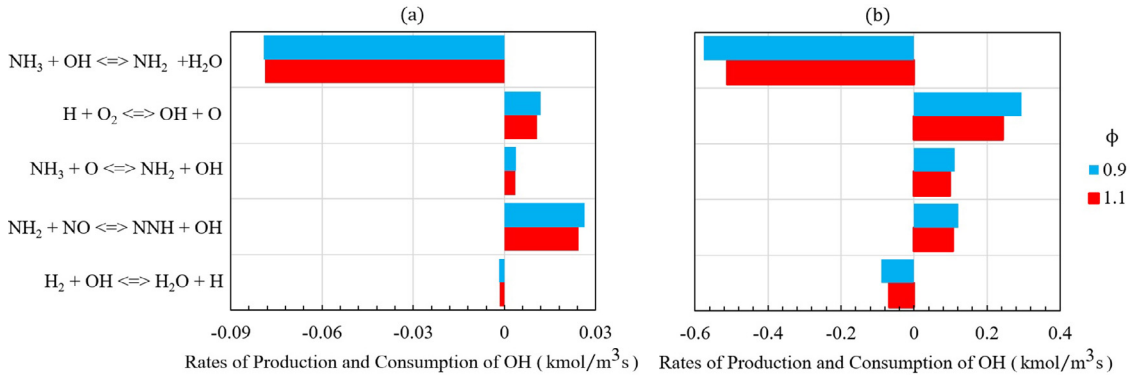

Fig. 11. Rates of consumption and production of OH radical in plasma-assisted $NH_3/O_2/N_2$ combustion for T_{in} = 850 K and ϕ = 0.9 and 1.1 with *PRF* = 50 kHz, *E/N* = 350 Td, and (a) E_p = 5 mJ/cm^3 and (b) E_p = 15 mJ/cm^3.

the main source of OH production, increases by a factor of 3 when N_2 is replaced by He. This is in the order of the ratio of the IDT of plasma-assisted NH_3/O_2/He to that of $NH_3/O_2/N_2$ mixtures with E_p = 5 mJ/cm^3, i.e., 2, which can be found in Fig. 6. It should be noted that the quenching reaction of the electronically excited N_2 with NH_3 directly dissociate the fuel via $N_2(A)+NH_3 \rightarrow N_2+H+NH_2$ reaction, while the quenching reactions of electronically excited He, i.e., He*, with NH_3 result in ionized species, i.e., NH_3^+, NH_2^+, NH^+, and H radical. To further evaluate the effects of such reactions on plasma-assisted combustion, simulations were performed for plasma-assisted stoichiometric NH_3/O_2/He at T_{in} = 850 K assisted by 20 nanosecond plasma pulses with E_p = 5 mJ/cm^3 with and without considering the quenching reactions of He* with NH_3. It is found that the IDT and flame speed change by 5% and 0.6%, when such reactions are neglected in the simulations.

Two zoom-ins shown in Fig. 6, depict the different responses of IDT, depending on the range of E_p, as follows. For low and medium E_p values, e.g., E_p < 7 mJ/cm^3, the IDT weakly depends on ϕ, similar to the non-plasma cases. Interestingly, contrary to this trend, the plasma is more effective in assisting lean mixtures in terms of IDT at high E_p values, e.g., E_p > 7 mJ/cm^3. Fig. 11 shows the production and consumption rates of OH radical under different equivalence ratios and pulse energy densities calculated over 20 pulses of the plasma discharge. At low pulse energy densities, $NH_2+NO \leftrightarrow NNH+OH$ is the main source of the OH radical, while $H + O_2 \leftrightarrow OH+O$ plays the key role in producing OH at high E_p values. Such differences in the main route of OH radical production can be explained by examining the pathways of H radical plotted in Fig. 12. Here, the pathways are obtained over 20 pulses of plasma. The results show that $H + O_2+M \leftrightarrow HO_2+M$ and $HNO+H \leftrightarrow NO+H_2$ compete with $H + O_2 \leftrightarrow OH+O$ chain branching reaction for H radical at low pulse energy density values, which lowers the direct OH radical production via $H + O_2 \leftrightarrow OH+O$. This in turn impels the OH radical production to the other alternative route, i.e., $NH_2+NO \leftrightarrow NNH+OH$. Such competitions are considerably incidental at high E_p values. Fig. 11 also shows that, in all the cases, OH radical is mainly consumed during the thermal phase to dissociate the fuel into NH_2. The equivalence ratio has negligible effects on the production and consumption rates of OH radical at low pulse energy density values, which results in an insignificant impact of the equivalence ratio on IDT at low pulse energy density values, as observed in Fig. 6. However, increasing the pulse energy density amplifies the rates of production and consumption of OH radical, as it can be found in Fig. 11, being more pronounced for ϕ = 0.9 than ϕ = 1.1. This is because O_2 is abundant under the lean conditions, which facilitates OH production via $H + O_2 \leftrightarrow OH+O$. This trend is analogous to the effects of preheating reported in previous non-plasma studies showing that lean ammonia flames are more sensitive to the increase of the initial mixture temperature as compared to the stoichiometric and moderately rich ones [19].

The question posed here concerns the precise contribution of plasma in assisting lean and rich mixtures. To address this, plasma energy branching is computed during a single plasma pulse discharged in lean and rich mixtures. The results and the path fluxes of a selected number of species are presented in Fig. 13. The main differences between the selected cases, i.e., ϕ = 0.9 and 1.1, are that the percentage of the energy used to excite and ionize O_2 and N_2 is higher in the lean mixture than that in the rich mixture, since more O_2 and N_2 molecules exist in the lean mixture as those in the rich one. In a similar way, the energy taken by the reactions to excite NH_3 is higher in the rich mixture than that in

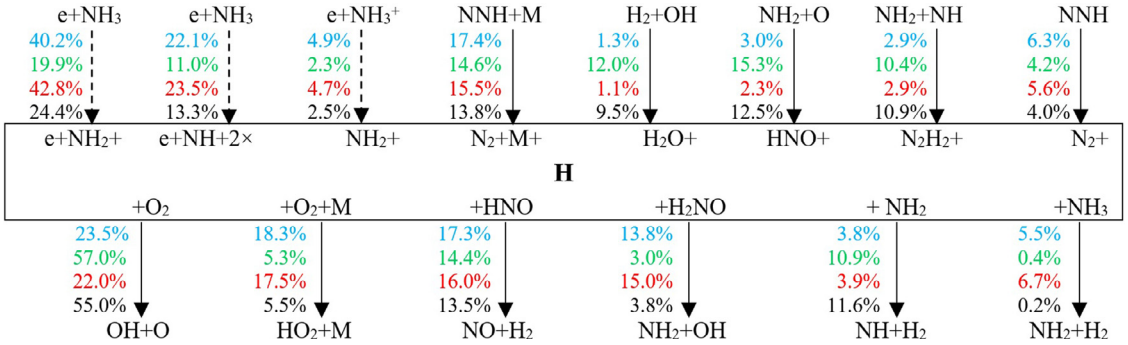

Fig. 12. Path fluxes of H radical in plasma (dashed-arrows) and thermal (arrows) phases in plasma-assisted $NH_3/O_2/N_2$ combustion for $\phi = 0.9$ and $E_p = 5$ mJ/cm^3 (blue), $\phi = 0.9$ and $E_p = 15$ mJ/cm^3 (green), $\phi = 1.1$ and $E_p = 5$ mJ/cm^3 (red), $\phi = 1.1$ and $E_p = 15$ mJ/cm^3 (black) and $T_{in} = 850$ K with $PRF = 50$ kHz and $E/N = 350$ Td. (For interpretation of the references to color in this figure legend, the reader is referred to the web version of this article.)

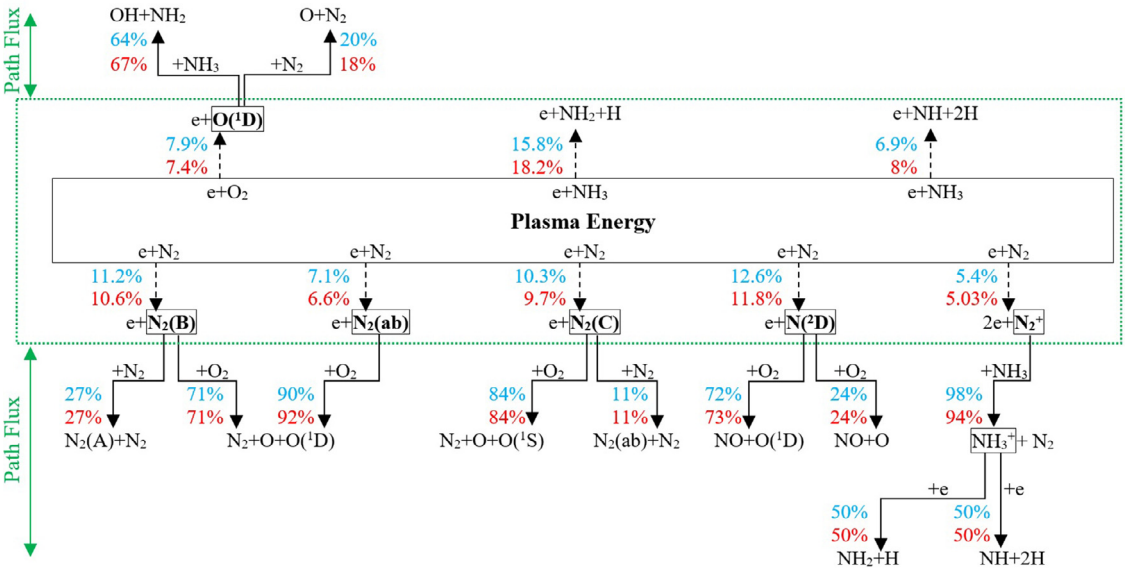

Fig. 13. Distribution of the plasma energy (dashed-arrows) as well as the consumption path flux (arrows) of a selected number of species (enclosed by rectangles) in $NH_3/O_2/N_2$ mixtures for $T_{in} = 850$ K, $\phi = 0.9$ (blue) and $\phi = 1.1$ (red) assisted by a plasma pulse with $PRF = 50$ kHz, $E_p = 15$ mJ/cm^3 and $E/N = 350$ Td. (For interpretation of the references to color in this figure legend, the reader is referred to the web version of this article.)

the lean one due to the abundant concentration of NH_3 in the rich case. The more energy used to excite and ionize the oxidizer, the more $O(^1D)$, $N_2(B)$, $N_2(ab)$, $N_2(C)$, $N_2(D)$, and NH_3^+ active plasma species, which subsequently take part in reactions to form O, OH, NH_2, H, NH radicals, as shown in Fig. 13. On the other hand, the higher energy taken to the excitation reaction of NH_3, the more NH_2, NH, and H radicals. The above analyses show that more OH radicals should be directly generated by the plasma discharge in lean mixtures than that in rich mixtures. In order to justify this, the maximum value of OH radical generated in a single plasma pulse with $E_p = 15$ mJ/cm^3 discharged in $NH_3/O_2/N_2$ at $T_{in} = 850$ K was measured for both lean and rich cases. It is found that plasma generates 183 and 170 ppm of OH radical in lean and rich mixtures, respectively. Therefore, besides the superior thermal effects under the lean condition addressed before by Han et al. [19], the plasma discharges also contribute to the observed higher enhancements in IDT achieved under the lean condition as those under the rich and stoichiometric cases, shown in Fig. 6.

4.3. Effects of NSD on laminar flame structure

4.3.1. Flame speed and thickness

Fig. 14 shows the laminar flame speed of ammonia at $T_{in} = 850$ K as a function of E_p in lean, stoichiometric and rich mixtures. Both multi-component diffusion and radiation heat losses effects were considered in the calculations. The results show that using NSD with $E_p > 10$ mJ/cm^3 increases the laminar flame speed of ammonia by an order of magnitude. These effects are more pronounced in the lean mixture, which is consistent with the details presented in the previous section.

Fig. 15 shows the laminar flame thickness of $NH_3/O_2/N_2$ and $NH_3/O_2/He$ as a function of E_p and ϕ. The flame thickness is defined as $(T_b - T_u)/(dT/dX)_{Max.}$, where T_b is the temperature of burned gases, T_u is the temperature of fresh reactants, and $(dT/dX)_{Max.}$ is the maximum temperature gradient through the flame [34]. Unlike the flame speed (see Fig. 14), results show that the flame thickness is a non-monotonic function of E_p. For each ϕ, there exists a unique E_p, the critical value (shown by E_{pm} in Fig. 15), at which the flame thickness takes its minimum. The trend at low E_p values is analogous to the effects of the mixture temperature on the flame thickness. The higher the mixture temperature, the thinner the flame. Depending on the equivalence ratio, E_{pm} is in the range of 12–15 mJ/cm^3. Such effects are further examined by analyzing the inner structure of the flame in Fig. 16, showing the profiles of heat release rate across the flame. Fig. 16 also includes the profile of the heat release rate across a highly preheated flame of $T_{in} = 1500$ K, to clarify the differences between the heat release rates of a plasma-assisted flame and a highly preheated non-

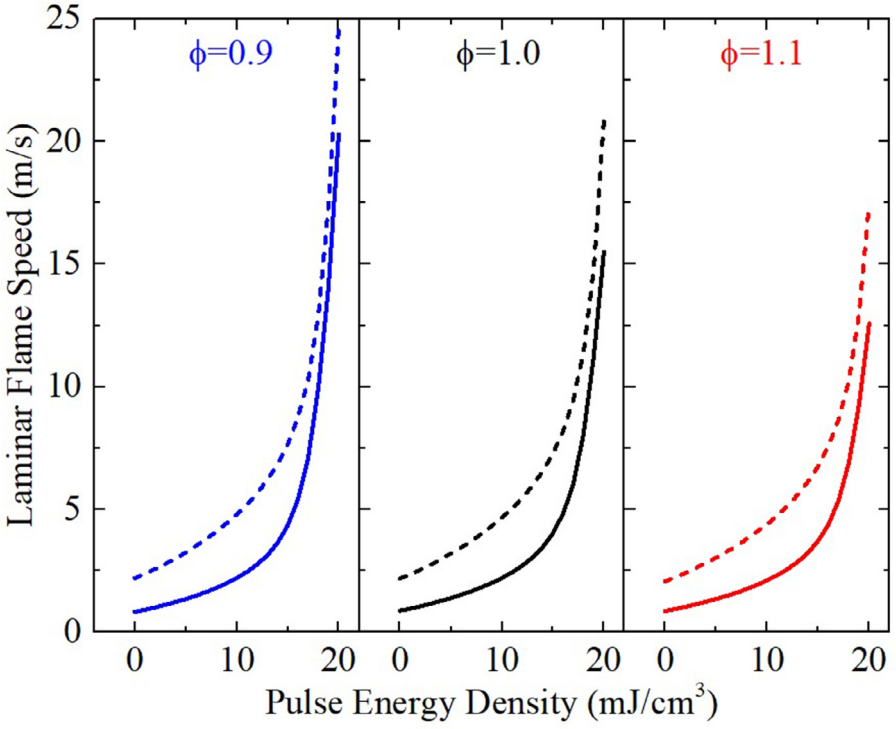

Fig. 14. Laminar flame speed of $NH_3/O_2/N_2$ (solid lines) and NH_3/O_2/He (dash lines) as functions of E_p and ϕ for T_{in} = 850 K with *PRF* = 50 kHz and *E/N* = 350 Td.

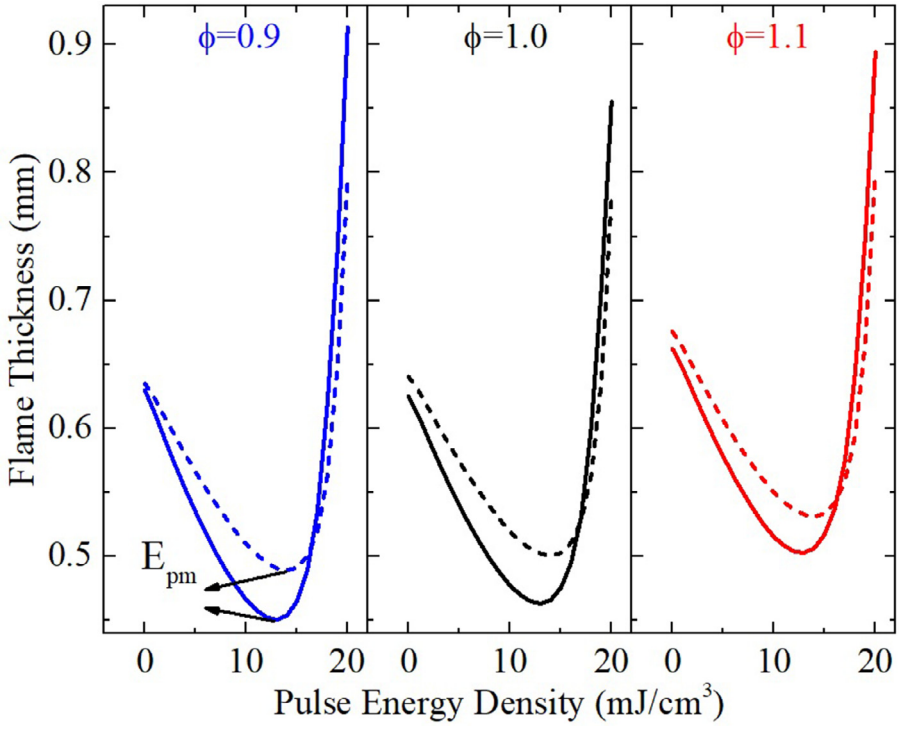

Fig. 15. Laminar flame thickness of $NH_3/O_2/N_2$ (solid lines) and NH_3/O_2/He (dash lines) as functions of E_p and ϕ for T_{in} = 850 K with *PRF* = 50 kHz and *E/N* = 350 Td.

plasma flame. In Fig. 16, the spatial location involves an offset to ensure the location of maximum heat release at the origin in all cases. The results show that for low E_p values, e.g., $E_p\langle$ 5 mJ/cm^3, the flame structure is virtually identical to the non-plasma and highly preheated cases, namely, the preheating zone does not involve any significant heat release. However, at high E_p values, e.g., E_p = 20 mJ/cm^3, the heat release across the flame is shifted toward the preheat zone, explaining the increase in the flame thickness observed for $E_p\rangle E_{pm}$ in Fig. 15. Such a broadening of the heat release profile is comparable to the well-distributed reaction zone in flameless combustion mode, with significant implications for the turbulent flame regime [35]. It is worth noting that the well-distributed reaction zone is the key characteristic of flameless combustion mode, which results in low temperature gradients

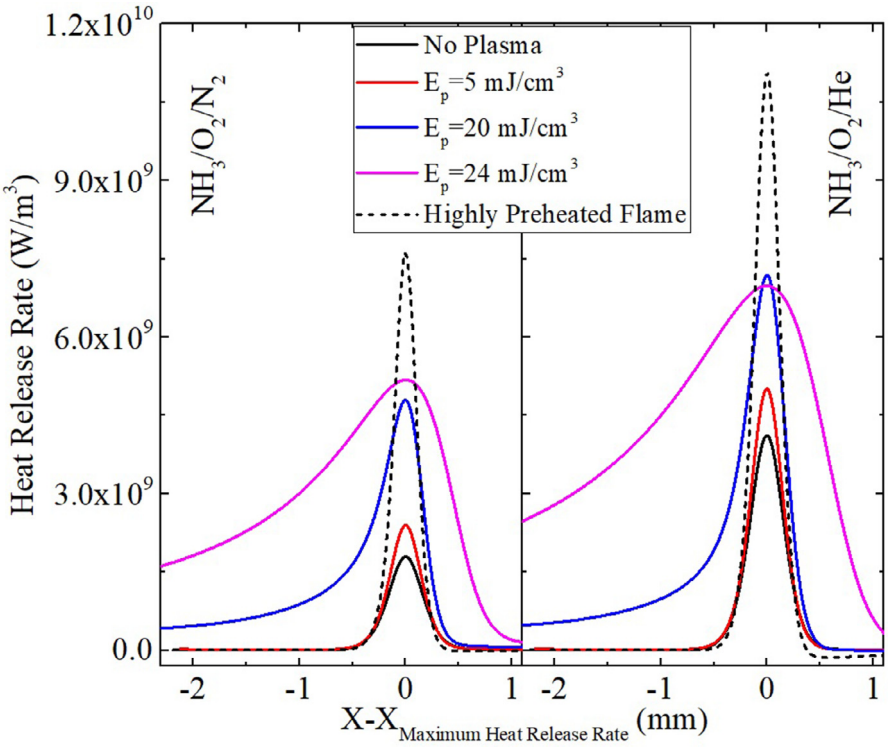

Fig. 16. Laminar flame structure of $NH_3/O_2/N_2$ (left) and NH_3/O_2/He (right) as functions of E_p for T_{in} = 850 K with *PRF* = 50 kHz and *E/N* = 350 Td.

and low NOx emissions [35]. Further investigations are mandatory to quantify the effects of E_p on the regime of combustion and its implication in the modeling of plasma-assisted turbulent premixed flame.

4.3.2. NOx emissions

The NOx emissions of the studied cases are plotted in Fig. 17, which are determined at 6 cm downstream of the flame. In Fig. 17, the NOx levels are adjusted to the reference 15% O_2 level. In all cases, NO_X emissions initially rise as E_p increases. However, there is a certain value, E_{pc}, at which NO_X emissions tend to reach their peak values, beyond which further increases in E_p decrease the NOx emissions. Fig. 17 shows that E_{pc} is larger as the mixture gets richer. The non-monotonic trend of NOx emissions as a function of E_p is a result of competing processes controlling the production and consumption of NO, as is elaborated in Fig. 18 showing rates of consumption and production of NO for $NH_3/O_2/N_2$ mixture at T_{in} = 850 K with *PRF* = 50 kHz and *E/N* = 350 Td. Increasing E_p accelerates the overall consumption rate of fuel-originated species, e.g., NH_2, and thus NO_X formation. Fig. 18 supports this by showing that increasing the pulse energy density, considerably raises the production rate of NO, specifically through HNO+H↔NO+H_2, NH_2+O↔H_2+NO, and NH+O_2↔NO+OH reactions. The other dichotomy process is the reburning of the nitrogen oxides mostly in reactions with NH_2 and NH radicals, i.e., NH_2+NO↔NNH+OH, NH_2+NO↔N_2+H_2O, NH+NO↔N_2O+H. In rich flames, NH_2 and NH radicals are naturally predominant, leading to lower NO_X emissions. In such cases, higher values of E_p are required to produce more NH_2 and NH radicals as compared to the intrinsic levels in a flame not affected by the plasma discharge to increase the consumption rate of NO.

4.3.3. Preheating

It is of both practical and fundamental interest to evaluate the plasma potential in assisting combustion under engine-like conditions, specifically during a cold start-up. To address this, Fig. 19(a) shows the percentage increase from the laminar flame speed of the non-plasma $NH_3/O_2/N_2$ ($S_{L\text{-}NP}$) to the laminar flame speed by using

NSD ($S_{L\text{-}P}$) at ϕ = 0.8–1.2 and T_{in} = 298–1000 K. The results show that the nanosecond plasma discharge with E_p = 5 mJ/cm^3 can increase the flame speed of ammonia by over 40% at T_{in} = 298 K. Such flame speed enhancements are more noticeable under the lean condition as compared with stoichiometric and rich mixtures as discussed above. Anyhow, the results show that preheating has considerable effects on plasma-assisted ammonia combustion. For instance, the percentage increase in the flame speed rises from 35% to 76% in the stoichiometric mixture as the mixture temperature is elevated from 298 to 1000 K. To compare the effects of pure preheating with those of plasma discharge on ammonia combustion, the required preheat temperature (ΔT) was calculated for $NH_3/O_2/N_2$ at ϕ = 0.8–1.2 to achieve the same level of enhancements in the flame speed without using plasma discharges as the ones presented in Fig. 19(a). The results plotted in Fig. 19(b) show that relatively low preheat temperatures are needed to gain a similar percentage increase in the flame speed of $NH_3/O_2/N_2$ at low T_{in} values assisted by 20 nanosecond plasma pulses with E_p = 5 mJ/cm^3. However, the required ΔT for a similar flame speed enhancement as that achieved by using plasma discharges increases considerably when T_{in} is elevated. For instance, preheating the stoichiometric $NH_3/O_2/N_2$ mixture at T_{in} = 850 K with ΔT = 149 K results in a similar flame speed enhancement as that attained by discharging 20 nanosecond plasma pulses. It should be noted that in Fig. 19(a) the pulse energy density was kept constant at 5 mJ/cm^3. Obviously, the more pulse energy density, the higher required preheat temperature to achieve an identical enhancement in the flame speed by relying on just preheating. For instance, stoichiometric $NH_3/O_2/N_2$ mixture at T_{in} = 850 K should be preheated by 310 K and 549 K to rise the flame speed of stoichiometric $NH_3/O_2/N_2$ mixture to those achieved by discharg-

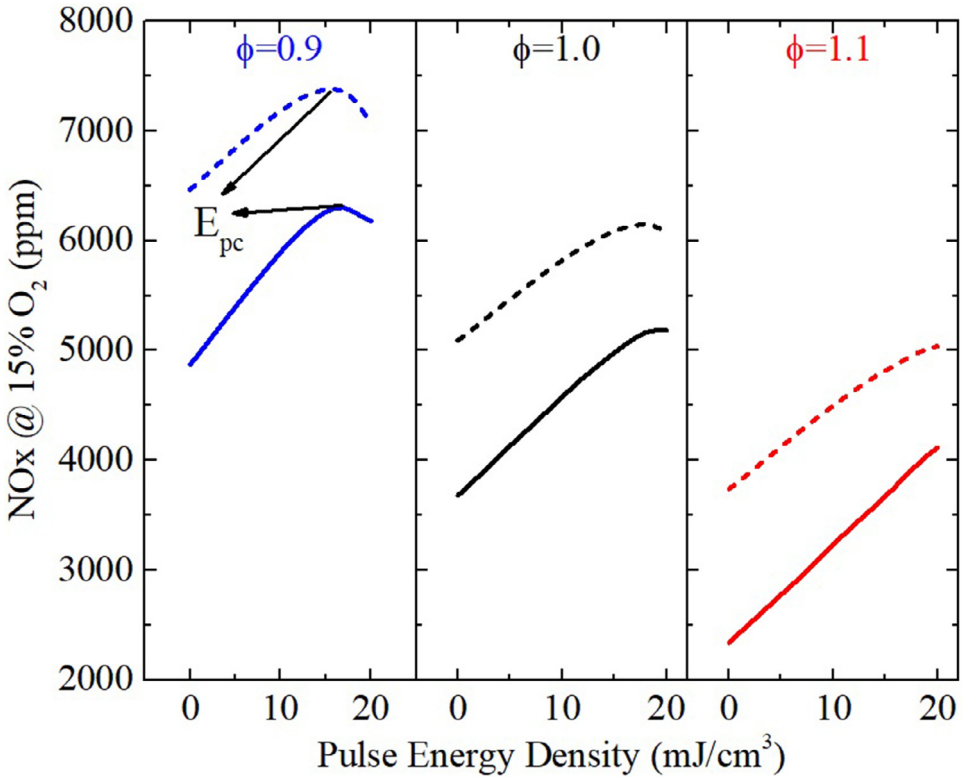

Fig. 17. NOx emissions of plasma-assisted $NH_3/O_2/N_2$ (solid lines) and NH_3/O_2/He (dash lines) flames as functions of E_p and ϕ for T_{in} = 850 K with *PRF* = 50 kHz and *E/N* = 350 Td.

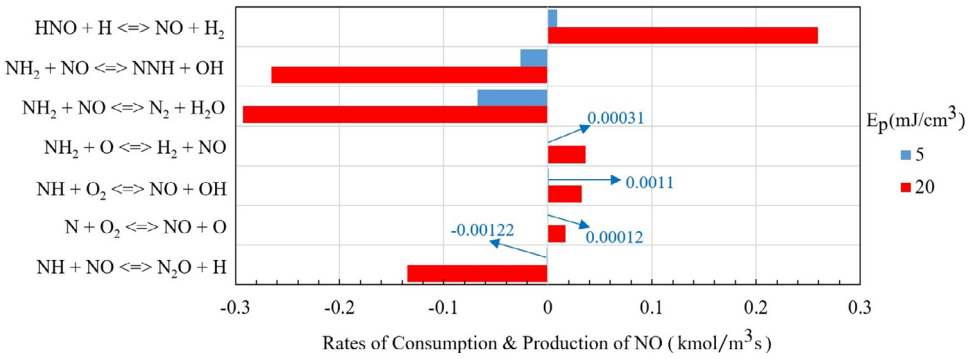

Fig. 18. Rates of consumption and production of NO in plasma-assisted $NH_3/O_2/N_2$ combustion for T_{in} = 850 K and ϕ = 0.9 with *PRF* = 50 kHz and *E/N* = 350 Td.

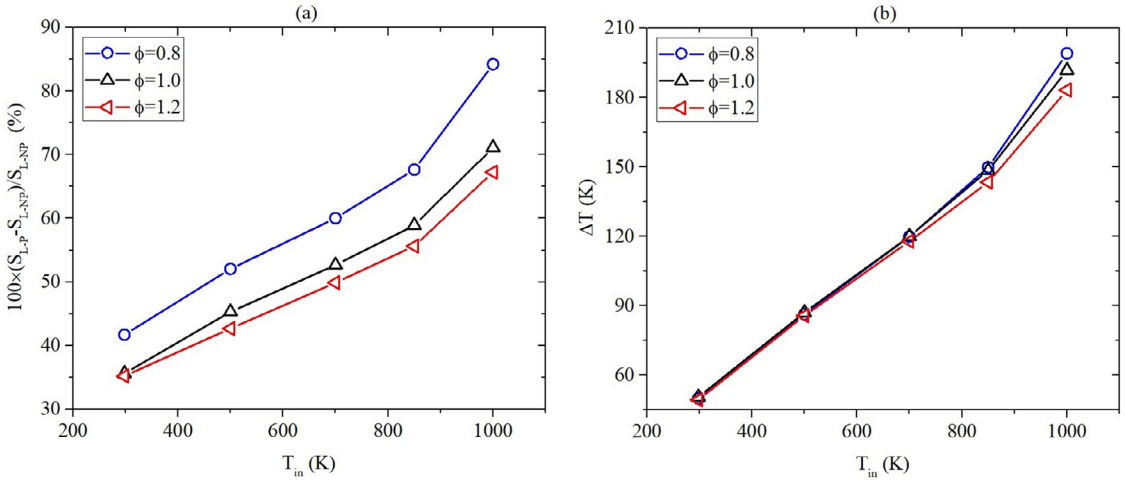

Fig. 19. (a) Percentage increase in $NH_3/O_2/N_2$ flame speed as a function of initial temperature for ϕ = 0.8, 1, 1.2 with *PRF* = 50 kHz, *E/N* = 350 Td, E_p = 5 mJ/cm^3 and (b) required preheat temperature without using plasma discharges to achieve similar enhancement in the flame speed as those presented in subfigure a. (For interpretation of the references to color in this figure legend, the reader is referred to the web version of this article.)

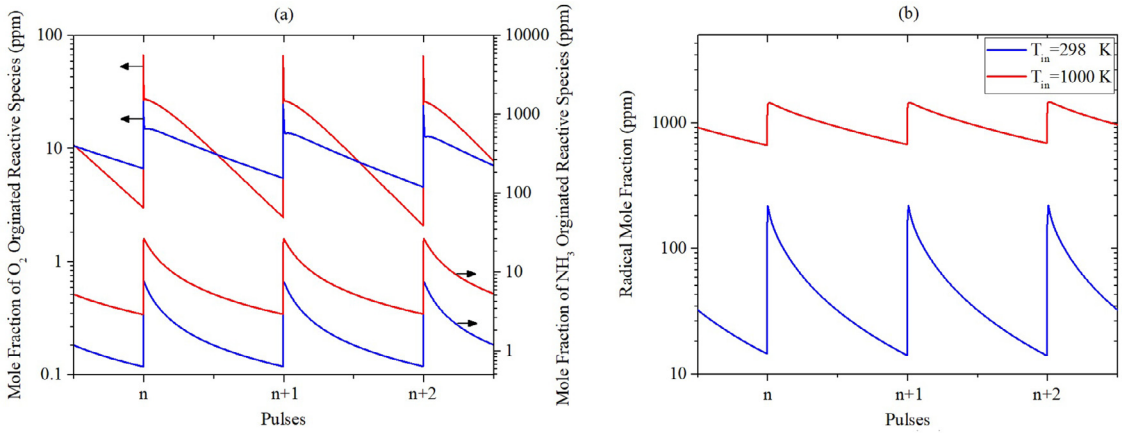

Fig. 20. Time evolution of mole fractions of (a) electronically excited and charged species and (b) radicals in plasma-assisted $NH_3/O_2/N_2$ combustion for $\phi = 1.0$ with $E_p = 5$ mJ/cm^3, $PRF = 50$ kHz, and $E/N = 350$ Td.

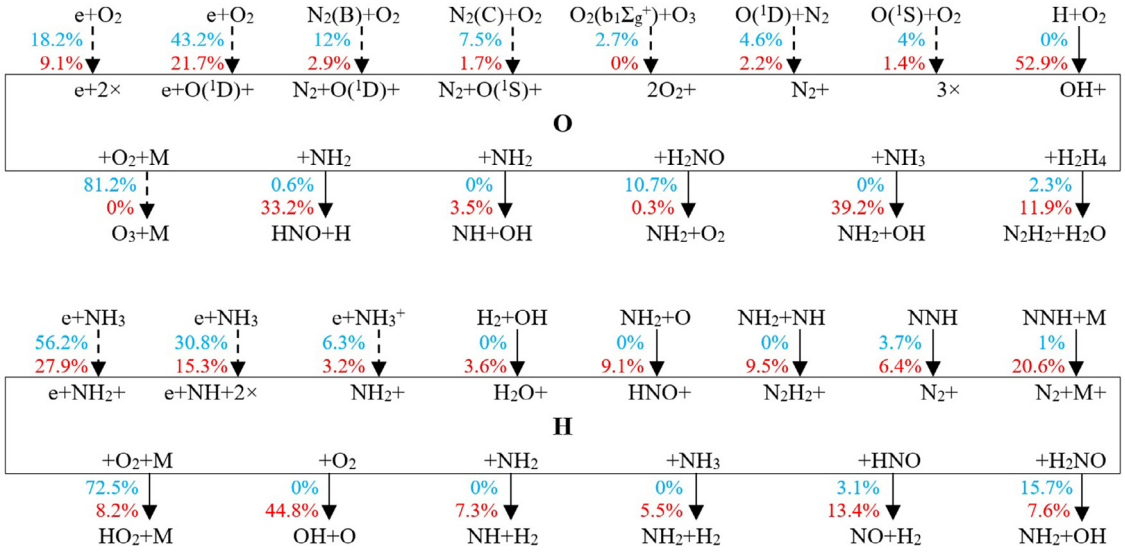

Fig. 21. Path fluxes of O (top) and H (bottom) in plasma (dashed-arrows) and thermal (arrows) phases in plasma-assisted stoichiometric $NH_3/O_2/N_2$ for $T_{in} = 298$ K (blue) and $T_{in} = 1000$ K (red) with $E_p = 5$ mJ/cm^3, $PRF = 50$ kHz, and $E/N = 350$ Td. (For interpretation of the references to color in this figure legend, the reader is referred to the web version of this article.)

ing 20 nanosecond plasma pulses with $E_p = 10$ and 15 mJ/cm^3, respectively.

Analyses of the fate of the key species controlling plasma-assisted combustion were performed, to further examine the effects of initial mixture temperature on plasma-assisted ammonia combustion. Fig. 20 shows the temporal distribution of mole fraction of reactive plasma species originating from NH_3 and O_2 alongside the radicals, calculated by taking the summation of the mole fractions of {NH_3^+, NH_2^+, NH^+}, {$O_2(a^1\Delta_g)$, $O_2(b^1\Sigma_g^+)$, O_2^+, O_2^*, $O(^1D)$, $O(^1S)$, O^+}, and {H, O, NH, NH_2}, respectively. The results show that preheating the mixture in plasma-assisted combustion significantly increases reactive plasma species and radical mole fractions. Fig. 21 shows the path fluxes of O and H radicals obtained over 20 plasma pulses with $E_p = 5$ mJ/cm^3, $PRF = 50$ kHz, and $E/N = 350$ Td for $NH_3/O_2/N_2$ mixture at $T_{in} = 298$ and 1000 K. The results show that O radical is mainly produced in the plasma phase in the low-temperature case. At higher mixture temperatures, most of the O radical, i.e., 52.9%, is generated in the thermal phase via H + $O_2 \leftrightarrow$OH+O chain branching reaction. The results also show that the main part of the O radical, i.e., 81.2%, in the low-temperature case converts into ozone via an endothermic third body reaction. The path flux of ozone, presented in the Supplementary Material, shows that 80% of the produced O_3 in the low-temperature case completely converts back into O_2 and O via $O_2(b^1\Sigma_g^+)+O_3 \rightarrow 2O_2+O$. Contrary to this, O radical in the high-temperature case contributes to the fuel consumption reactions to produce NH_2, HNO, H, and OH radicals.

Fig. 21 also shows that plasma is the main source of H radical in the cold mixture, i.e., 96.1%, while in the high-temperature case, 53.1% of H radical is produced in the thermal phase. The H radical is solely consumed in the thermal phase in all cases, during which H + $O_2 \leftrightarrow$OH+O and H + O_2+M$\leftrightarrow HO_2$+M play the key role in consuming H radical in low and high-temperature cases, respectively. The pathway analyses of HO_2 radical for $T_{in} = 298$ K, presented in the Supplementary Material, show that over 55% of HO_2 radical takes part in NO+$HO_2 \leftrightarrow NO_2$+OH and NH_2+$HO_2 \leftrightarrow H_2$NO+OH reactions to directly produce OH radical. Here, sensitivity analyses are carried out to further assess the contribution of H + $O_2 \leftrightarrow$OH+O and H + O_2+M$\leftrightarrow HO_2$+M reactions to changing OH radical pools under low and temperature conditions. Fig. 22 shows the spatial distribution of the normalized sensitivity coefficien of OH mole fraction along the one-dimensional freely propagating flame caused by changing the pre-exponential factor of the above-mentioned reactions. In Fig. 22, the spatial location involves an off-

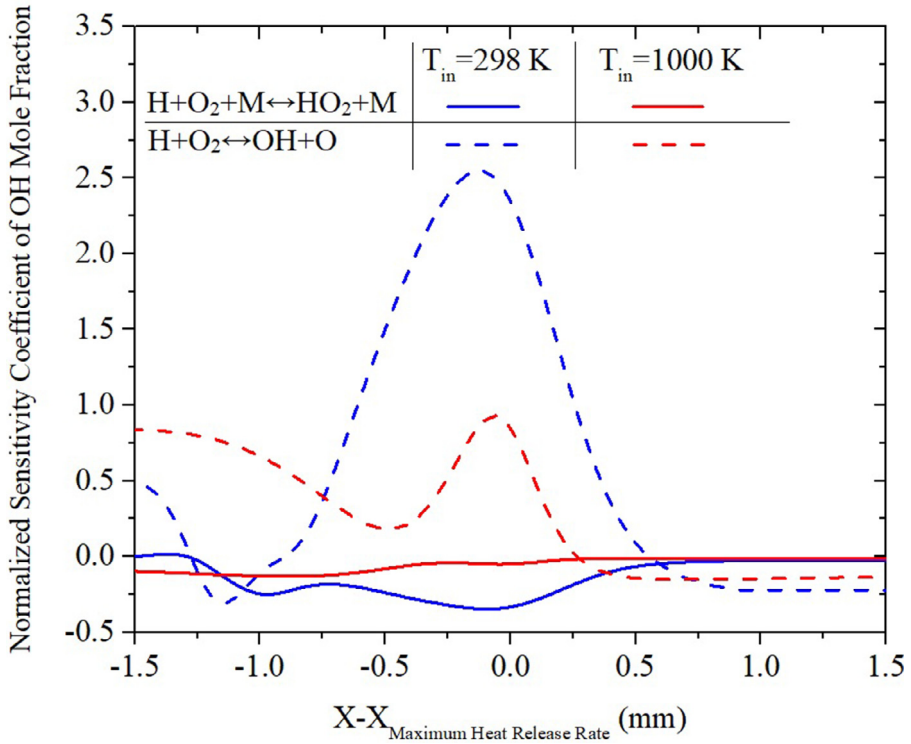

Fig. 22. Normalized sensitivity coefficient of OH mole fraction along the laminar flame caused by changing the pre-exponential factors of the selected reactions for plasma-assisted stoichiometric $NH_3/O_2/N_2$ for T_{in} = 298 K and T_{in} = 1000 K with E_p = 5 mJ/cm^3, *PRF* = 50 kHz, and *E/N* = 350 Td.

set to ensure the location of maximum heat release at the origin in all cases. The results show that the magnitude of the normalized coefficient is relatively smaller for H + O_2+M↔HO_2+M than that for H + O_2↔OH+O, since the latter reaction contributes directly to the production of OH radical. However, the aim of the present analyses is to find the overall contribution of each reaction to the production of OH radical by comparing the sign of the coefficients. Obviously, the H + O_2↔OH+O reaction plays a significant role in raising the OH radical pool near the flame front being more pronounced under low initial temperature conditions. Interestingly, contrary to this, the H + O_2+M↔HO_2+M reaction has a negative impact on OH radical production. The negative value of the normalized sensitivity coefficient shows that increasing the path flux through this path, lowers the OH radical production. Therefore, shifting the H radical consumption pathway from H + O_2↔OH+O to H + O_2+M↔HO_2+M by reducing the initial mixture temperature, results in less OH radical production and subsequently weak plasma effects on combustion characteristics, e.g., flame speed, as is shown in Fig. 19.

5. Conclusions

The effects of nanosecond plasma discharge on ammonia combustion under various pulse energy densities, reduced electric fields, and thermophysical conditions were investigated by coupling ZDPlasKin and Cantera open-source codes. The assembled kinetic model includes the excitations, ionizations, quenching, recombination, charge exchanges, and neutral state reactions for $NH_3/O_2/N_2$/He mixtures. Moreover, a non-uniform time step method was used to accurately resolve multi-time-scale chemical reactions in plasma-assisted ammonia combustion.

Analyses revealed that ignition delay time and laminar flame speed of ammonia/air respond non-monotonically to the reduced electric field, being maximum at the medium ranges of the reduced electric field. At low reduced electric field values, the major part of the plasma energy is used to excite the diluent to higher vibrational levels, which have trivial impacts on ammonia combustion. On the other hand, plasma discharges with a high reduced electric field activate ionization reactions of the diluent, which lowers O and OH radical productions. It was shown that unlike the non-plasma or low-energy plasma-assisted cases, the ignition delay time with high-energy plasma discharges, e.g., E_p > 10 mJ/cm^3, drops when the equivalence ratio of the mixtures is decreased. This is attributed to the higher rates of production and consumption of OH in lean mixtures as compared with stoichiometric and fuel-rich mixtures. The results showed that NSD produces more reactive plasma species during the pulses when N_2 is replaced by He in the oxidizer, thanks to the strengthened NH_3 and O_2 ionization reactions in NH_3/O_2/ He as that in $NH_3/O_2/N_2$. It was also shown that increasing the mixture temperature enhances the plasma performance.

In terms of the effects of plasma on the flame structure, it was observed that the flame thickness non-monotonically depends on the pulse energy density. For all the equivalence ratios examined here, there is a certain pulse energy density at which the flame attains its minimum thickness. Further increases in the pulse energy density tend to disrupt the flame structure by broadening the heat releases rate profile, and substantial increases in the flame thickness toward a reactive preheat zone structure.

Declaration of Competing Interest

None.

Acknowledgments

This study as a part of PlasNH3 project was supported by Marie Sklodowska-curie Foundation through MSCA-IF-EF-ST action, H2020-MSCA-IF-2020 call. AAK is grateful to the Knut and Alice Wallenberg Foundation for the financial support through grant

KAW2019.0084 COCALD. Cardiff University gratefully acknowledges the support from the Welsh European Funding Office through “Flexible Integrated Energy Systems”, project 80835.

Supplementary materials

Supplementary material associated with this article can be found, in the online version, at doi:10.1016/j.combustflame.2022.112368.

References

[1] H. Kobayashi, A. Hayakawa, K. Kunkuma, A. Somarathne, E. Okafor, Science and technology of ammonia combustion, Proc. Combust. Inst. 37 (1) (2019) 109–133.
[2] A. Valera-Medina, F. Amer-Hatem, A. Azad, I. Dedoussi, M. de Joannon, R. Fernandes, P. Glarborg, H. Hashemi, X. He, S. Mashruk, J. McGowan, C. Mounaim-Rouselle, A. Ortiz-Prado, A. Ortiz-Valera, I. Rossetti, B. Shu, M. Yehia, H. Xiao, M. Costa, Review on ammonia as a potential fuel: from synthesis to economics, Energy Fuels 35 (9) (2021) 6964–7029.
[3] A. Starikovskiy, N. Aleksandrov, Plasma-assisted ignition and combustion, Prog. Energy Combust. Sci. 39 (1) (2013) 61–110.
[4] G. Faingold, J. Lefkowitz, A numerical investigation of NH_3/O_2/He ignition limits in a non-thermal plasma, Proc. Combust. Inst. 38 (4) (2021) 6661–6669.
[5] G. Faingold, O. Kalitzky, J. Lefkowitz, Plasma reforming for enhanced ammonia-air ignition: a numerical study, Fuel Commun. 12 (100070) (2022) 1–9.
[6] S. Yang, S. Nagaraja, W. Sun, V. Yang, Multiscale modeling and general theory of non-equilibrium plasma-assisted ignition and combustion, J. Phys. Condens. Matter 50 (43) (2017) 1–18.
[7] Y. Ju, W. Sun, Plasma assisted combustion: progress, challenges, and opportunities, Combust. Flame 162 (3) (2015) 529–532.
[8] W. Sun, S. Won, T. Ombrello, C. Carter, Y. Ju, Direct ignition and S-curve transition by in situ nano-second pulsed discharge in methane/oxygen/helium counterflow flame, Proc. Combust. Inst. 34 (1) (2013) 847–855.
[9] Y. Wang, P. Guo, H. Chen, Z. Chen, Numerical modeling of ignition enhancement using repetitive nanosecond discharge in a hydrogen/air mixture I: calculations assuming homogeneous ignition, J. Phys. Condens. Matter 54 (6) (2020) 1–11.
[10] T. Casey, J. Han, M. Belhi, P. Arias, F. Bisetti, H. Im, J. Chen, Simulations of planar non-thermal plasma assisted ignition at atmospheric pressure, Proc. Combust. Inst. 36 (3) (2017) 4155–4163.
[11] T. Taneja, S. Yang, Numerical modeling of plasma assisted pyrolysis and combustion of ammonia, AIAA SciTech Forum, Virtual Event, 2021.
[12] J. Choe, W. Sun, T. Ombrello, C. Carter, Plasma assisted ammonia combustion: simultaneous NOx reduction and flame enhancement, Combust. Flame 228 (2021) 430–432.
[13] Q. Lin, Y. Jiang, C. Liu, L. Chen, W. Zhang, J. Ding, J. Li, Controllable NO emission and high flame performance of ammonia combustion assisted by non-equilibrium plasma, Fuel 319 (123818) (2022).
[14] G. Kim, J. Park, S. Chung, C. Yoo, Effects of non-thermal plasma on turbulent premixed flames of ammonia/air in a swirl combustor, Fuel 323 (124227) (2022).
[15] Y. Tang, D. Xie, B. Shi, N. Wang, S. Li, Flammability enhancement of swirling ammonia/air combustion using AC powered gliding arc discharges, Fuel 313 (122674) (2022).
[16] P. Johnson, T. Taneja, S. Yang, Global pathway analysis of plasma assisted ammonia combustion, AIAA SciTech Forum, San Diego, 2022.
[17] S. Pancheshnyi, B. Eismann, G. Hagelaar, L. Pitchford, Computer code zdplaskin, University of Toulouse, LAPLACE, CNRS-UPS-INP, Toulouse, France, 2008.
[18] D. Goodwin, R. Speth, H. Moffat and B. Weber, "Cantera: an object-oriented software toolkit for chemical kinetics, thermodynamics, and transport processes," Version 2.5.1, 2021.
[19] X. Han, Z. Wang, Y. He, Y. Liu, Y. Zhu, A. Konnov, The temperature dependence of the laminar burning velocity and superadiabatic flame temperature phenomenon for NH3/air flames, Combust. Flame 217 (2020) 314–320.
[20] A. Konnov, On the role of excited species in hydrogen combustion, Combust. Flame 162 (2015) 3753–3770.
[21] H. Zhong, X. Mao, A. Rousso, C. Patrick, C. Yan, W. Xu, Q. Chen, G. Wysocki, Y. Ju, Kinetic study of plasma-assisted n-dodecane/O2/N2 pyrolysis and oxidation in a nanosecond-pulsed discharge, Proc. Combust. Inst. 38 (4) (2021) 6521–6531.
[22] "Dutton database," www.lxcat.net, December 13, 2021.
[23] S. Nagaraja, W. Sun, V. Yang, Effect of non-equilibrium plasma on two-stage ignition of n-heptane, Proc. Combust. Inst. 35 (3) (2015) 3497–3504.
[24] T. Ombrello, S. Won, Y. Ju, S. Williams, Flame propagation enhancement by plasma excitation of oxygen. Part I: effects of O3, Combust. Flame 157 (10) (2010) 1906–1915.
[25] X. Mao, Q. Chen, A. Rousso, T. Chen, Y. Ju, Effects of controlled non-equilibrium excitation on H2/O2/He ignition using a hybrid repetitive nanosecond and DC discharge, Combust. Flame 206 (2019) 522–535.
[26] W. Sun, S. Won, T. Ombrello, C. Carter, Y. Ju, Direct ignition and S-curve transition by in situ nano-second pulsed discharge in methane/oxygen.helium counterflow flame, Proc. Combust. Inst. 34 (2013) 847–855.
[27] S. Nagaraja, T. Li, J. Sutton, I. Adamovich, V. Yang, Nanosecond plasma enhanced H2/O2/N2 premixed flat flames, Proc. Combust. Inst. 35 (2015) 3471–3478.
[28] J. Lefkowitz, P. Guo, A. Rousso, Y. Ju, Species and temperature measurements of methane oxidation in a nanosecond repetitively pulsed discharge, Philos. Trans. R. Soc. A 373 (20140333) (2015).
[29] I. Adamovich, M. Nishihara, I. Choi, Energy coupling to the plasma in repetitive nanosecond pulse discharges, Phys. Plasma 16 (2009) 113505.
[30] M. Uddi, N. Jiang, E. Mintusov, I. Adamovich, W. Lempert, Atomic oxygen measurements in air and air/fuel nanosecond pulse discharges by two photon laser induced fluorescence, Proc. Combust. Inst. 32 (2009) 929–936.
[31] J. Lefkowitz, P. Guo, A. Rousso, Y. Ju, Species and temperature measurements of methane oxidation in a nanosecond repetitively pulsed discharge, Philos. Trans. R. Soc. A 373 (2015).
[32] X. Mao, A. Rousso, Q. Chen, Y. Ju, Numerical modeling of ignition enhancement of CH4/O2/He mixtures using a hybrid repetitive nanosecond and DC discharge, Proc. Combust. Inst. 37 (2019) 5545–5552.
[33] R. Patel, C. Oommen, Influence of reduced electric field (E/N) on plasma-assisted low-temperature oxidation, J. Propul. Power 36 (2019) 235–247.
[34] C. Sun, C. Sung, L. He, C. Law, Dynamics of weakly stretched flames: quantitative description and extraction of global flame parameters, Combust. Flame 118 (1999) 108–128.
[35] A. Perpignan, A. Rao, D. Roekaerts, Flameless combustion and its potential towards gas turbines, Prog. Energy Combust. Sci. 69 (2018) 28–62.